Calibrating and testing the discrete element parameters for peanut seedling film

Qiangji Peng[1], Xin He[1,2], Guoming Li[1,3], Rusha Yang[4], Xiaoyu Wang[1], Chunyan Zhang[1], Ningning Zhang[1], Jianming Kang[1*]

(1. *Shandong Academy of Agricultural Machinery Sciences, Jinan 250100, China*;
2. *School of Mechanical and Automotive Engineering, Liaocheng University, Liaocheng 252000, Shandong, China*;
3. *College of Agricultural Engineering and Food Science, Shandong University of Technology, Zibo 255012, Shandong, China*;
4. *Shandong Provincial Department of Agriculture and Rural Affairs, Jinan 250013, China*)

Abstract: This study constructed a numerical model using the discrete element software EDEM to address the current lack of calibrated contact parameters for peanut seedling membranes and the absence of precise simulation model parameters for mechanized separation. The Hysteretic Spring Contact Model (HSCM) was employed to calibrate the contact parameters of peanut seedling membranes. The angle of repose of peanut seedling membranes was determined through image processing combined with the least squares method. Through central composite design (CCD), a second-order response model linking the contact parameters to the angle of repose was established. Optimization was achieved by using the angle of repose obtained from physical tests as the objective. Secondary simulation tests were conducted with the calibrated parameters, revealing a relative error of 1.37% between the simulated and physical angles of repose. This confirmed the effectiveness of the parameters in calibrating peanut seedling membrane characteristics. The findings offer theoretical and empirical support for discrete element simulations of peanut seedling membrane separation and peanut straw pulverization processes.

Keywords: discrete element method, peanut, post-crumbled seedling film, angle of repose, contact parameters, calibration
DOI: 10.25165/j.ijabe.20241705.9087

Citation: Peng Q J, He X, Li G M, Yang R S, Wang X Y, Zhang C Y, et al. Calibrating and testing the discrete element parameters for peanut seedling film. Int J Agric & Biol Eng, 2024; 17(5): 65–72.

1 Introduction

Peanut holds significant importance as both an oilseed and cash crop in China, consistently ranking among the world's top two in terms of planting area and total output[1]. Post-harvest, peanut straw, also known as peanut seedlings, emerges as a valuable byproduct of peanut production, boasting rich nutritive value. This resource can effectively substitute certain high-quality protein feeds and roughage, thus aiding in the reduction of feed costs[2]. Despite the widespread adoption of peanut mulching cultivation techniques, which have notably enhanced both yield and quality, a persistent issue arises in the form of film residue. This residue comprises a mixture of recycled peanut straw, residual film soil, and other impurities, collectively termed as the seedling film. The entanglement of straw and residual film complicates separation processes, rendering the crushed peanut straw unsuitable for direct forage processing. Consequently, the utilization of peanut straw forage is significantly hindered[3].

Traditionally, the removal of residual film from peanut seedling film entails the use of a kneader, yet this method presents challenges such as incomplete separation and low efficiency[4]. Accurately simulating and analyzing the separation process of seedling film mixtures hinges upon the rational configuration of contact parameters for peanut seedling film. While physical tests can yield material contact parameters, measurement errors often arise due to various factors including test conditions, environmental influences, equipment variations, and operator proficiency levels. Such inaccuracies can undermine the precision of simulation model construction and numerical simulations. Therefore, with advancements in computing capabilities and the evolution of simulation software, the discrete element method has gained prominence within the agricultural domain.

Recent studies have employed the discrete element method to model and calibrate various agricultural materials. For instance, Liao et al.[5] utilized single orb particles to model oilseed rape stalks in three dimensions, refining parameters for a stalk crushing discrete element simulation model. Liu et al.[6] developed a discrete element model for maize stover, addressing significant differences in the mechanical properties of its outer skin and inner flesh through a bilayer bonded bimodal distribution model. Tian et al.[7] focused on parameter calibration for maize stover-soil mixtures, while Zhang et al.[8] tackled the issue of uneven crushing of banana straw by calibrating its bonding parameters. Zhang et al.[9] utilized the Hertz-Mindlin with Bonding contact model in EDEM to construct a maize stover model, aiming to calibrate the contact parameters between maize stover and the hammer blades of a kneading machine. Similarly, Zhao et al.[10] simulated shear, radial

Received date: 2024-05-20 **Accepted date:** 2024-09-13
Biographies: Qiangji Peng, PhD, research interest: agricultural machinery and equipment and intelligent control, Email: pengqiangji@shandong.cn; **Xin He**, MS, research interest: intelligent agricultural machinery, Email: 3054505842@qq.com; **Guoming Li**, MS, research interest: agricultural machinery and equipment, Email: 1466719941@qq.com; **Rusha Yang**, BS, research interest: extension of agricultural mechanization technology, Email: 1470179542@qq.com; **Xiaoyu Wang**, MS, research interest: agricultural machinery and equipment, Email: wangxiaoyusdut@163.com; **Chunyan Zhang**, MS, research interest: agricultural machinery and equipment, Email: sdnjyzcy@163.com; **Ningning Zhang**, MS, research interest: agricultural machinery and equipment, Email: ning0716@126.com.

***Corresponding author: Jianming Kang**, PhD, research interest: agricultural machinery and equipment and key technologies. Shandong Academy of Agricultural Machinery Sciences, Jinan 250100, China. Tel:+86-15624389451, Email: kjm531@sina.com.

compression, and tensile characteristic tests of a discrete elemental mechanical model of rice straw. Ma et al.[11] conducted DEM simulations based on the Hertz-Mindlin contact model for crop straw within a variable amplitude screen box, concluding that this method effectively resolves retention issues with agricultural materials. Furthermore, Maraldi et al.[12] performed compression tests on rice straw, examining the impact of bale density and orientation on the mechanical properties of straw bales. Leblicq et al.[13] proposed a novel simulation model for wheat straw, capable of replicating the bending behavior of crop stalks under stress. This comprehensive model accounts for geometry, material properties, and external loading of crop stems, simulating the deformation and damage processes of straw using a discrete element method. Sadrmanesh et al.[14] developed a numerical simulation model for the tensile properties of plant fibers using the discrete element method (DEM), successfully calibrating key parameters such as tensile strength and Young's modulus. Additionally, Kattenstroth et al.[15] employed multiball bonding in EDEM to model straw, enabling simulation and analysis of the cutting process.

While existing literature by both domestic and foreign scholars has extensively constructed straw models for various crops and conducted significant research on calibrating their contact parameters, limited attention has been directed towards simulating and calibrating parameters for peanut seedling film mixtures. This paper addresses this gap by focusing on peanut seedling membranes as the research subject. Through experimentation, a simulation model is constructed, employing the injection method to stack peanut seedling membranes. Image processing techniques are then utilized to extract boundaries, and the least-squares method is employed to fit angles. Subsequently, discrete element simulation of peanut seedling membranes is conducted via CCD tests, followed by parameter calibration. The accuracy of the model is validated through physical tests.

2 Materials and methods

The primary test material was peanut seedling film sourced from Rizhao City, Shandong Province, with the peanut seedling variety being Hanyu 25. The experiment was conducted in February 2024 at the pilot plant of the Shandong Academy of Agricultural Machinery Science. Key equipment utilized during the testing process included a standard test sieve with a diameter ranging from 0 to 20 mm, a YP-B electronic balance (Hangzhou Comirey Instrument Equipment Co., Ltd，China) with 0.01 g accuracy, JMB5003 electronic scales (China Qingdao Chenfei Environmental Protection Technology Co., Ltd, China) with 0.001 g accuracy, a DHS-20A electronic fast moisture tester (Shanghai Bangxi Technology Co., Ltd, China) with 0.001 g quality accuracy and 0.01% moisture content accuracy, digital vernier calipers, an injection method angle of repose test device, among others.

2.1 Test materials and angle of repose tests

Peanut seedling film was randomly sampled in 10 groups, each weighing 2000 g. From each group, 500 g was further sampled using the quadrature method. Moisture content was measured using an electronic rapid moisture tester, followed by manual removal of entangled film for weighing and determination of residual film proportion in the samples. In order to ensure the effectiveness of the angle of repose test, the peanut seedling film was crushed and pretreated according to the actual work requirements. Subsequently, a standard test sieve with a diameter of 0-20 mm was used for sieving (refer to Figure 1), with the basic parameters of peanut seedling film outlined in Table 1.

a. Source material b. Sieve material

Figure 1 Raw material and screening results

Table 1 Basic parameters of peanut seedling film

Sample	Water content/%	Grain stem distribution/%					Film content/%
		0-1 mm	1-2 mm	2-5 mm	5-10 mm	10-20 mm	
Post-seedling membrane	13.41±1.60	2.85	5.32	43.06	35.41	13.36	0.5-1.0

The angle of repose test was executed utilizing the injection method[16], employing an injection angle of repose tester (Xiamen Boshi Testing Equipment Co., Ltd., China). To ensure comprehensive test coverage across various scenarios, peanut seedling films with a particle size distribution of 2-10 mm, constituting 88.47% of the total, were selected for physical testing. Ten physical tests were conducted, and averages were computed to mitigate human error in the testing process. Following a resting period, a multi-angle photo of the pile was captured parallel to the pile using a cellphone. Subsequently, the edge contour information of the pile was extracted using the C++ programming language with the OpenCV open-source library (refer to Figure 2). The angle of repose of the peanut seedling membranes was then fitted using the least-squares method, yielding an angle of repose of 54.1°±1.6° for a water content of 13.41%±1.60% and a film content of 0.5%-1.0% peanut seedling membranes (2.1°).

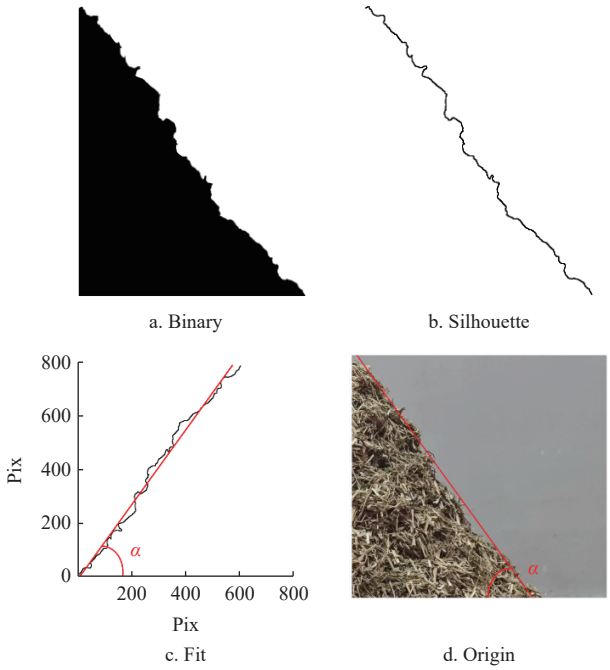

a. Binary b. Silhouette

c. Fit d. Origin

Figure 2 Image processing

2.2 Contact model selection

The primary constituent of peanut seedling membranes is peanut straw, characterized by a hollow structure possessing bulk material properties and compressibility. For discrete element simulation, the hysteretic spring contact model (HSCM) within the discrete element software is chosen as the contact model between peanut seedling membranes, augmented with linear cohesion model

(LCM) in its normal direction. HSCM is aptly suited for situations where particles undergo substantial pressures resulting in plastic deformations. The force-displacement relationship schematic diagrams and structural schematics are depicted in Figure 3.

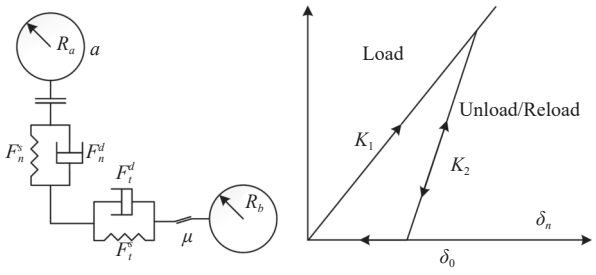

a. Schematic diagram of force-displacement relationship b. Schematic diagram of particle contact relationship

Note: R_a and R_b represent the radius of particles a and b, respectively, m; F_n^s and F_n^d denote the normal contact and damping forces, respectively, N; F_t^s and F_t^d denote the tangential contact and damping forces, respectively, N; μ is the coefficient of friction; δ_n denotes the normal overlap between particles, m; δ_0 denotes the residual overlap between particles, m; K_1 and K_2 denote the loading and unloading stiffnesses, respectively, N/m.

Figure 3 Hysteresis spring contact model

In the contact model, the normal force F_n^s between the particles can be expressed as follows:

$$F_n^s = \begin{cases} K_1\delta_n & (K_1\delta_n < K_2(\delta_n - \delta_0)) \\ K_2(\delta_n - \delta_0) & (\delta_n - \delta_0) \\ 0 & (\delta_n \le \delta_0) \end{cases} \tag{1}$$

$$K_1 = 5R^* \min(Y_a, Y_b) \tag{2}$$

where, R^* represents the equivalent radius of the two contacting particles, m; Y_a and Y_b denote the yield strength of the two particles, Pa. These parameters can be derived using Equation (3).

$$\begin{cases} Y = \dfrac{2E}{525\sqrt{R}} \\ R^* = \dfrac{R_a + R_b}{R_a R_b} \end{cases} \tag{3}$$

where, E represents the Young's modulus. If Y<100 Pa, 0.003E can be used as a substitute.

The residual overlap quantity δ_0 is updated as follows:

$$\delta_0 = \begin{cases} \delta_n\left(1 - \dfrac{K_1}{K_2}\right) & (K_1\delta_n < K_2(\delta_n - \delta_0)) \\ \delta_0 & (\delta_n - \delta_0) \\ \delta_0 & (\delta_n - \delta_0) \end{cases} \tag{4}$$

where, K_1 and K_2 represent the loading and unloading stiffnesses, respectively, N/m; δ_n denotes the normal overlap, and δ_0 denotes the residual overlap.

The coefficient of recovery e, damping coefficient b_n and stiffness coefficient γ_t between the contacting particles can be calculated as follows:

$$\begin{cases} e = \sqrt{\dfrac{K_1}{K_2}} \\ b_n = -\dfrac{F_n^d}{2v_n \ln e}\sqrt{\dfrac{\ln^2 e + \pi^2}{m^* K}} \\ \gamma_t = \dfrac{(F_t^d)^2(\ln^2 e + \pi^2)}{4v_t^2 m^* K \ln^2 e} \end{cases} \tag{5}$$

where, F_n^d and F_t^d represent linear normal and tangential damping forces, respectively, N; v_n and v_t represent the particle normal and tangential velocities of motion, m/s; m^* denotes the equivalent mass, $m^* = \dfrac{m_a + m_b}{m_a m_b}$, m_a and m_b denote the masses of particles a and b, respectively, kg; K represents either K_1 or K_2.

2.3 Simulation modeling of peanut seedling membrane

Spherical particles or assemblies composed of such particles are commonly employed in agriculture simulation studies[17]. Liu et al.[18] employed the center-stacking method to model maize stover through particle arrangement, while Niu et al.[19] directly spliced multiple spheres to model alfalfa stalks. Although the aforementioned test materials were cylindrical in shape, the modeling methods and constructed shapes varied significantly. Simplifying nearly cylindrical materials into clusters of spherical particles or units can reduce simulation time and modeling complexity. However, studies have indicated that overly simplistic simulation models may lead to substantial deviations in simulation results[20,21].

Before the simulation calibration test, angle of repose comparison tests were conducted using multiple modeling approaches to ascertain a reasonable method. Therefore, the peanut straw model with a diameter of 5 mm and a length of 10 mm was used for test comparison, and the relationship between different modeling methods and simulation time and simulation accuracy was analyzed, a reasonable simulation model was selected for multiple sets of tests, and the number of balls of the peanut straw model was 3, 4, 5, 7, 16, and 253 balls, respectively. The residual film accounted for approximately 2%, with a small area, which exhibited negligible influence on the angle of repose. The residual film was simplified and modeled, but no experimental comparison was carried out, as shown in Figure 4.

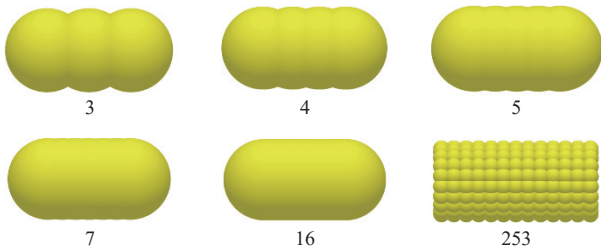

Figure 4 Comparison test simulation model

As the number of balls increased, the particles conformed more closely to the cylindrical shape. By employing 253 balls, the model refined the entire structure into multiple spheres to simulate the epidermal and hollow features of peanut straw. The test setup model was simplified in SolidWorks at a 1:1 scale for comparison tests. This simplified model was imported into EDEM, and dynamic production was utilized to establish a virtual plane above the funnel as a pellet plant with a filling quantity of 3000. The angle of repose of peanut straw was then simulated for comparison tests in the Hysteretic Spring Contact Model (HSCM) contact modeling simulation environment. Image processing techniques were employed to measure the angle. The EDEM simulation test is illustrated in Figure 5.

Bao et al.[22] and Yang et al.[23] assigned the coefficients of restitution, static friction, and rolling friction between peanut straw as 0.20, 0.50, and 0.20, respectively. For the coefficients between peanut straw and steel, they were set as 0.50, 0.50, and 0.01, respectively. These values were substituted into EDEM, with all other parameters kept constant. Each test was repeated five times in

each group, and the average value was computed. The relationship between angle of repose, number of balls, and simulation time is shown in Figure 6.

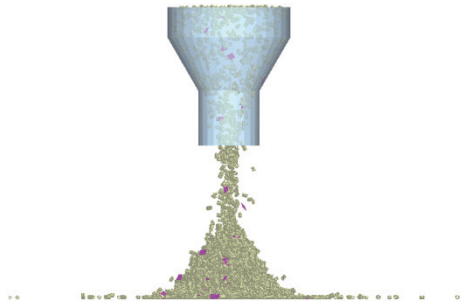

Figure 5 Schematic of the simulation

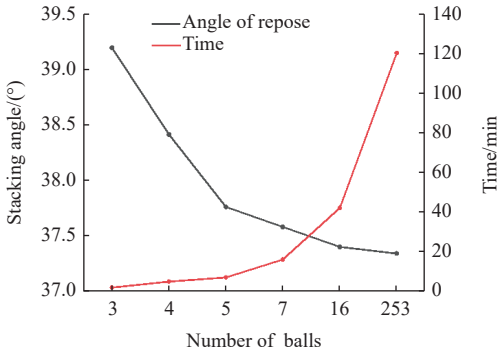

Figure 6 Angle of repose and time vs. ball count

As depicted in Figure 6, the angle of repose in the simulation test gradually diminishes with increasing modeling complexity. Notably, when the number of modeled balls exceeds 7, the curve begins to converge within a reasonable range. Specifically, a discrepancy of 0.18° is observed between 7 and 16 balls, and only 0.06° is observed between 16 and 253 balls. Additionally, the simulation time for 16 balls is 162.5% longer than for 7 balls, and the simulation time for 253 balls is 185.7% longer than for 16 balls. It follows that the more precise the model constructed, the greater the number of ball-to-ball contacts, enhancing the accuracy of the angle-of-rest simulation test albeit prolonging the simulation time.

Based on the aforementioned analysis, the construction of the peanut seedling film simulation model prioritizes the peanut straw component, given its predominant presence compared to residual film. By simplifying the modeling to account for the relatively smaller area of residual film, friction characteristics between model materials remain unaltered, thus ensuring simulation test accuracy while reducing computational load. Adopting a peanut straw particle size of 5 mm and a length 1.4 times its diameter (7 mm), coupled with a fixed length and width of 10 mm for the residual film, the XYZ coordinates of peanut straw and residual film model spheres were determined using C++. These coordinates were then imported to generate spherical particles at customized locations (refer to Figure 7). The peanut straw, featuring a 1-mm skin thickness, comprises 180 elementary particle units, while the residual film consists of 100 such units. For the simulation model, the radii of these elementary particle units are uniformly set at 0.5 mm. The peanut straw model varies in size from 0.5 to 1.5 times its actual dimensions, randomly generating a total of 8000 peanut straw models. Conversely, the residual film is generated at a fixed proportion of the total, resulting in 152 residual film models. Both materials are uniformly generated in a fixed ratio for angle of repose simulation tests conducted within a predetermined timeframe.

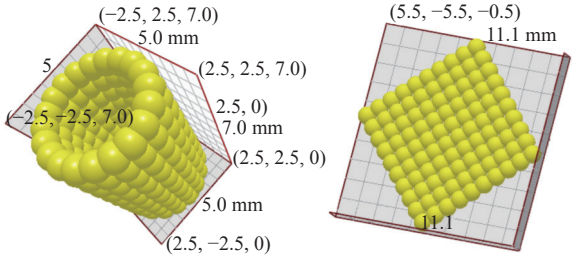

a. Peanut straw b. Residual film

Figure 7 Peanut seedling film simulation model

2.4 Calibration parameters and experimental design

Peanut seedling film predominantly comprises 98% peanut straws, wherein the contact parameters among peanut straws significantly influence the angle of repose of peanut seedling film. These parameters, designated as the test factor, were determined based on references[22,23] to establish the range of values for the coefficient of restitution (a), coefficient of static friction (b), and coefficient of rolling friction (c). Other parameters have minimal impact on the angle of repose and were set to intermediate values. The damping coefficients between particles in the HSCM model parameters and the stiffness coefficients adopted default values from EDEM software, namely 0.05 and 0.95, respectively[24,25]. The values of discrete element simulation parameters are outlined in Table 2.

Table 2 Discrete element simulation parameters

Sports event		Residual film	Stalk
Densities/kg·m^{-3}		164.68	230.00
Poisson's ratio		0.4076	0.3500
Shear modulus/MPa		8.962	1.000
Coefficient of restitution	Residual film	0.20	0.20-0.40
	Stalk	0.30	0.10-0.30
	Steel	0.10	0.50
Coefficient of static friction	Residual film	0.71	0.40-0.80
	Stalk	0.60	0.30-0.70
	Steel	0.71	0.50
Coefficient of rolling friction	Residual film	0.65	0.10-0.30
	Stalk	0.20	0.10-0.30
	Steel	0.65	0.01

A response surface test was designed using the principle of central combination design to ensure parameter reliability. The upper and lower limits of the parameter values in Table 2 were combined to formulate the response surface test. The test factor coding is illustrated in Table 3.

Table 3 Angle of repose simulation test factor coding

Code	Level		
	Coefficient of restitution (a)	Coefficient of static friction (b)	Coefficient of rolling friction (c)
–1.682	0.032	0.160	0.032
–1	0.100	0.300	0.100
0	0.200	0.500	0.200
1	0.300	0.700	0.300
1.682	0.370	0.840	0.370

Considering the influencing factors and their level values from Table 3, the combination optimization test method in quadratic regression orthogonal rotation was employed. Design-Expert 12.0.1 was utilized to process and analyze the test data, yielding the results of the peanut seedling membrane rest angle simulation test as listed in Table 4.

Table 4 Angle of repose simulation test design and results

Test No.	Code			Response value
	a	*b*	*c*	*y*
1	–1	–1	–1	39.94±2.46
2	1	–1	–1	39.82±2.01
3	–1	1	–1	40.79±2.75
4	1	1	–1	38.68±0.85
5	–1	–1	1	43.35±3.06
6	1	–1	1	47.73±2.25
7	–1	1	1	51.32±1.82
8	1	1	1	50.65±1.49
9	–1.682	0	0	41.97±1.57
10	1.682	0	0	45.69±0.72
11	0	–1.682	0	41.95±1.59
12	0	1.682	0	44.12±3.44
13	0	0	–1.682	40.39±0.86
14	0	0	1.682	53.72±2.43
15	0	0	0	46.71±1.82
16	0	0	0	47.56±2.67
17	0	0	0	46.41±1.52
18	0	0	0	46.71±1.82
19	0	0	0	45.89±1.00
20	0	0	0	44.69±2.20

3 Analysis of angle of repose test results

3.1 Analysis of test results

The peanut seedling film rest angle simulation test data was subjected to analysis of variance (ANOVA) using the analysis module in Design Expert 12.0.1 software (Stat-Ease, Inc, America) to establish a multiple regression equation for the peanut seedling film's rest angle and test its significance. The ANOVA results for the peanut seedling film are presented in Table 5.

Table 5 Quadratic analysis of variance results

Source	Sum of squares	Mean square	*F*-value	*p*-value
Model	312.9900	312.9900	30.9200	<0.0001**
a	4.3800	4.3800	3.9000	0.0766
b	14.8600	14.8600	13.2100	0.0046**
c	231.5600	231.5600	205.9000	<0.0001**
ab	6.2100	6.2100	5.5200	0.0406*
ac	4.4200	4.4200	3.9300	0.0754
bc	15.6300	15.6300	13.8900	0.0039**
a^2	14.0900	14.0900	12.5300	0.0054**
b^2	23.2600	23.2600	20.6800	0.0011**
c^2	0.3245	0.3245	0.2885	0.6029
Residual	11.2500	11.2500	--	--
Lack of fit	6.5600	6.5600	1.4000	0.3612
Pure error	4.6900	4.6900	--	--
Cor total	324.2400	324.2400	--	--
R^2=0.965; Adjusted R^2=0.934; Predicted R^2=0.82; CV=2.36%				

Note:** means extremely significant factor ($p\leq0.01$); * means significant factor ($0.01<p\leq0.05$); $p>0.05$ means non-significant factor; CV: Coefficient of vibration.

As indicated by the data in Table 5, the *p*-values of the primary terms *b* and *c* were <0.01, indicating their highly significant impact on the angle of repose. Conversely, the *p*-value of *a* was >0.05, suggesting its lack of significance in influencing the angle of repose. Previous studies have also highlighted that coefficients of static and rolling friction between particles are primary factors affecting the angle of repose[26-29]. The *p*-values for the interaction terms *ab*, *bc*, and *ac* were 0.0406, 0.0754, and 0.0039, respectively. Notably, *bc* significantly affected the angle of repose, while *ab* had a notable effect and *ac* did not. The *p*-values of the quadratic terms a^2 and b^2 were <0.01, signifying their high significance, whereas the *p*-value of c^2 was 0.6029, indicating its lack of significance. Eliminating insignificant influences, the degree of influence on the angle of repose was ranked in descending order: *c*, b^2, *bc*, *b*, a^2, and *ac*.

Based on the regression ANOVA results, the model coefficients' *p*-value is <0.0001, indicating a highly significant relationship between the independent and dependent variables described by the model. The misfit term's *p*-value, 0.3612, was considerably greater than 0.05, suggesting a well-fitted equation. The coefficient of variation (CV) at 2.36% was less than 10%, affirming the test's high reliability. The multivariate correlation coefficient R^2, the modified multivariate correlation coefficient R^2_{adj}, and the predicted multivariate correlation coefficient R^2_{pre} of the second-order response model were 0.9653, 0.9341, and 0.8201, respectively. All three values were close to 1, implying adequate explanation of the process by the fitted equations and good accuracy of the model. The precision (Adeq precision) at 19.981 was substantially higher than 4, indicating the model's good accuracy. The above data demonstrate that the regression model was well-adapted, with predicted values fitting well with physical test values. Factors *a*, *b*, and *c* exhibited a high degree of explanation for the response value *y*, and the second-order response model better predicted and optimized the angle of repose of peanut seedling membranes under varying conditions. Based on the regression ANOVA results and coding factors, a second-order response model between the contact parameters of peanut seedling membranes and angle of repose was obtained as shown in Equation (6):

$$y = 46.34 + 0.567a + 1.04b + 4.12c - 0.88ab + 0.74ac + 1.40bc - 0.99a^2 - 1.27b^2 + 0.15c^2 \quad (6)$$

3.2 Single-factor term impact analysis

In analyzing the trend of a single factor's influence on the angle of repose, denoted as *y*, the level values of the remaining two test factors were fixed at 0. The influence patterns of the coefficient of recovery, static friction coefficient, and rolling friction coefficient on the angle of repose *y* are illustrated in Figure 8.

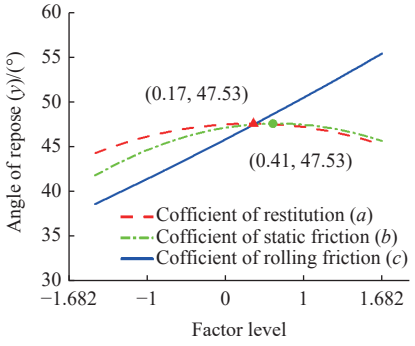

Figure 8 Relationship between single factors and angle of repose

As indicated by the curve direction in Figure 8, as the horizontal value of the coefficient of restitution *a* increased from –1.682 to 0.170, the angle of repose *y* increased continuously, reaching a peak value of 47.53° at *a*=0.17. Subsequently, as *a* increased from 0.170 to 1.682, *y* gradually decreases. In other words, as the recovery coefficient increased from 0.032 to 0.370, *y* initially increases and then decreased. The recovery coefficient can

be defined as the ratio of separation velocity to approach velocity of two objects along the direction normal to the contact point before and after collision[30]. Following a collision, particles possess some initial velocity and tend to drift outward from the contact position. Most particles accumulated after coming to a stop, especially given the non-standard cylindrical structure of peanut straw and its rough, less mobile surface, leading to a large angle of repose. As the recovery coefficient increased further, the kinetic energy lost in collisions decreased, making collisions more elastic. Consequently, particles attain greater initial velocity, dispersing widely and hindering pileup formation, resulting in a smaller angle of repose. Similar conclusions were drawn by Wu et al.[31] in their study on the angle of repose of clayey soils with varying recovery coefficients. The curves in the figure indicate that the effect of the recovery coefficient on the angle of repose is not significant. From a microscopic perspective, peanut straw, being a hollow structure, experiences compression after collision, leading to substantial kinetic energy loss and minimal velocity changes, hence its insignificant effect on the angle of repose.

The effect of the static friction coefficient *b* on the angle of repose aligned with that of the coefficient of recovery *a*, albeit with a more pronounced increase. The angle of repose *y* experienced growth as *b* ranged from –1.682 to 0.410, peaking at 47.53° when *b*=0.41. Subsequently, *y* steadily decreased as *b* continued to increase within the range of 0.410 to 1.682. Thus as the static friction coefficient increased from 0.16 to 0.84, *y* exhibited an initial increase followed by a decrease. With an increase in the coefficient of static friction between particles, inter-particle friction intensified, necessitating greater force to overcome the friction, impeding particle mobility, and fostering stable stacks, thereby increasing the angle of repose. This phenomenon was also elucidated by Liu et al.[32] in their study on contact parameters of large particle urea. As the coefficient of static friction between particles continues to increase, the pressurization of peanut straw generated elastic force, which, coupled with friction, led to a critical state inducing sliding of the pile body, thus initiating a gradual decrease in the angle of repose.

The influence of the rolling friction coefficient *c* on the response value exhibited a different pattern compared to the aforementioned influences, and *y* exhibited high sensitivity to it, steadily increasing as *c* levels increased. Thus, *y* exhibited continuous growth as the coefficient of rolling friction increased from 0.032 to 0.370. During particle falling and stacking, initial formation of a small stack occurred in the central region, with subsequent particles covering the outer layer. With a low rolling friction coefficient, the outer particles exhibited high rotational kinetic energy and weak inhibition of rotational moment of inertia, resulting in spreading to the boundary and forming a small angle of repose. However, as the coefficient of rolling friction between particles increased, the rotational kinetic energy of outer particles decreased, hindering rolling diffusion and promoting stacking in the height direction (i.e., the *Z*-axis direction), thus leading to a larger angle of repose. Similar explanations for the mechanism of the coefficient of kinetic friction's action in analyzing the angle of repose size have been provided by Laing et al.[33], Peng et al.[34], and Liu et al.[32]

3.3 Interaction term impact analysis

The significance analysis of the angle of repose of peanut seedling membrane revealed that the values of the interaction terms *ab* and *bc* were 0.0406 and 0.0039, respectively, while the value of the interaction term *ac* was 0.0754, indicating that the effects of *ab* and *bc* were significant. To further analyze the effects of interaction terms *ab* and *bc* on the angle of repose *y*, the maximum angle of repose was explored, as shown in Figures 9 and 10.

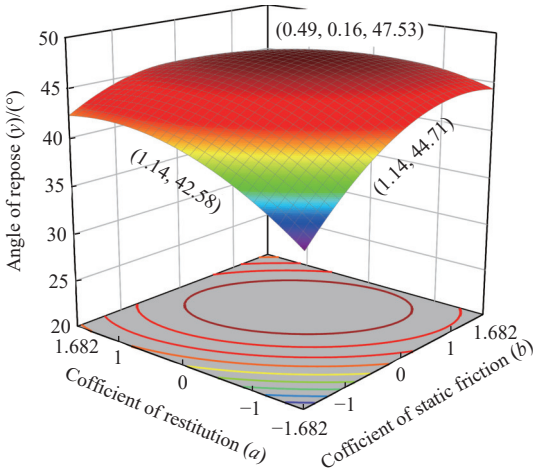

Figure 9 Effects of *ab* on angle of repose

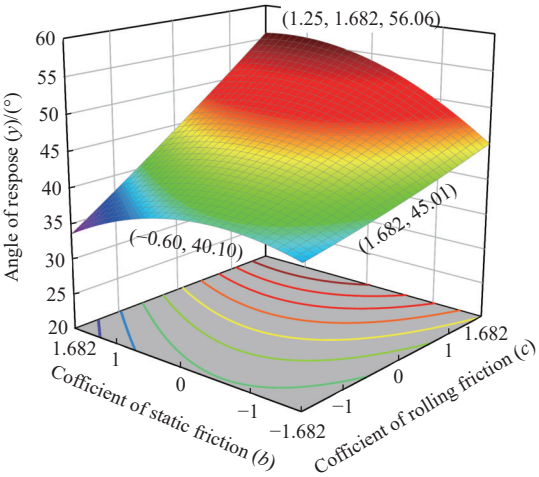

Figure 10 Effects of *bc* on angle of repose

3.3.1 Interaction term ab impact analysis

As shown in Figure 9, the overall graph exhibited a hill shape with a prominent peak and gentle slopes. The angle of repose *y* attained its highest value of 47.53° when the coefficient of restitution *a*=0.49 and the coefficient of static friction *b*=0.16.

The horizontal value of the coefficient of static friction *b* was held constant at –1.682, while the horizontal value of the coefficient of restitution *a* increased from –1.682 to 1.140, resulting in a continuous increase in the angle of repose *y*. Subsequently, as the horizontal value of *a* increased from 1.140 to 1.682, *y* decreased, reaching its maximum value of 42.58° at a horizontal value of *a* of 1.140. Conversely, as the horizontal value of *b* gradually increased to 1.682, the overall direction of *y* remained unchanged.

The value of *y* increased when the horizontal value of the coefficient of restitution *a* was fixed at –1.682, and the horizontal value of the coefficient of static friction *b* increased from –1.682 to 1.140. Then, as *b* increased from 1.140 to 1.682, *y* decreased, with its maximum value of 44.71° attained at a horizontal value of *b* of 1.140. Similarly, with the horizontal value of *a* changing to 1.682, the overall trend of *y* remained consistent.

Considering the synergistic effect of the coefficient of recovery *a* and the coefficient of static friction *b*, as the level values of both factors simultaneously increased from –1.682 to 1.682, *y* initially

increased to a peak, stabilized within a certain range, and then began to decrease. The range of values of the level values of a and b resulting in an increasing angle of repose y was wider than that resulting in a decreasing angle of repose. The binary regression equation comprising the test influences a, b, and the interaction term ab can be given by Equation (7):

$$y_{ab} = 46.34 + 0.57 \times a + 1.04 \times b - 0.8812 \times ab - 0.99 \times a^2 - 1.27 \times b^2 \quad (7)$$

3.3.2 Interaction term bc impact analysis

As depicted in Figure 10, the overall graph exhibited a skewed shape with higher values on the right and lower values on the left. The angle of repose y reaches its maximum value of 56.06° when the coefficient of static friction b=1.250 and the coefficient of rolling friction c=1.682.

The horizontal value of the static friction coefficient b was held constant at –1.682, while the horizontal value of the rolling friction coefficient c increased from –1.682 to 1.682. During this range, the angle of repose y exhibited a gradual increasing trend, peaking at 45.01° when the horizontal value of c was 1.682. As the level factor b gradually increased to 1.682, the upward trend of y became more pronounced.

Conversely, y increased when the horizontal value of the coefficient of rolling friction c was fixed at –1.682, and the horizontal value of the coefficient of static friction b increases from –1.682 to –0.600. Then, y decreased as b increased from –0.600 to 1.682, with its maximum value of 40.10° reached at a horizontal value of b of –0.600. As the level factor c gradually increased, the trend of y changed from increasing to decreasing, then to steady increase followed by another decrease. This pattern shifted in response to the influence of the primary term b on y.

Considering the combined effect of the coefficient of static friction b and the coefficient of rolling friction c, y exhibited a consistent upward trend as both factors simultaneously increased from –1.682 to 1.682. The binary regression equation comprising the test influence factors b and c, along with the interaction term bc, is represented by Equation (8):

$$y_{bc} = 46.34 + 1.04 \times b + 4.12 \times c + 1.04 \times bc - 1.27b^2 + 0.15 \times c^2 \quad (8)$$

3.4 Numerical fitting and experimental validation

The established second-order response model correlating contact parameters with the angle of repose of peanut seedling membranes was validated experimentally. This involved using the angle of repose measured in physical tests as the target value and employing the optimization module in Design-Expert software to fit this target value, while maintaining other parameters unchanged from the previous calibration. Objective and conditional constraint equations were established as depicted in Equation (9):

$$\begin{cases} y_{(2-10\,\mathrm{mm})} = \beta(53.1 \pm 2.1)^\circ \\ 0.1 < a < 0.3 \\ 0.3 < b < 0.7 \\ 0.1 < c < 0.3 \end{cases} \quad (9)$$

Using Equation (9), the contact parameters were derived, including the recovery coefficient, static friction coefficient, and rolling friction coefficient of peanut seedling membranes post-calibration. These parameters were then used as boundary conditions for verification simulations in EDEM software (refer to Figure 11). Angular information was extracted using the least-squares method based on image processing, with each experiment repeated three times to calculate the average values. The contact parameters and simulation results of the optimized peanut seedling membrane section are summarized in Table 6.

a. Test result b. Simulation results

Figure 11 Comparison chart of simulation results

Table 6 Calibration parameters and results

a	b	c	Simulation results	Test results	Inaccuracies
0.23	0.67	0.3	53.37°±1.65°	54.10°±2.10°	1.37%

The simulated angle of repose β of peanut seedling membranes, under conditions of 13.41%±1.60% water content, 0.5% to 1.0% film content, and 2-10 mm particle size distribution, was determined to be 53.37°±1.65°. This value exhibited a minor deviation of 1.37% compared to the actual physical test value. These results validate the feasibility of the parameters, thereby providing valuable reference for research on peanut seedling membrane separation devices.

4 Conclusions

1) Based on physical experiments, the film content and moisture content of peanut seedling film were determined to be in the ranges of 0.5%-1.0% and 13.41%±1.60%, respectively. The particle size distribution of the peanut seedling film was primarily within the 2-10 mm range. Under these conditions, the accumulation of peanut seedling film in the 2-10 mm interval was obtained using the injection method. The angle of repose boundary was fitted and extracted using the least squares method, implemented through C++-OpenCV. Experimental results indicated that the angle of repose for peanut seedling film under these conditions was 54.1°±2.1°

2) A comparative test of particle modeling was conducted using the HSCM contact model in EDEM software. The effects of different model construction methods on simulation accuracy and time were analyzed to determine the optimal approach. Additionally, models for peanut straw and simplified residual film were established.

3) Building upon the results of the CCD test, a second-order response model between contact parameters and the angle of repose of peanut seedling membrane was established. Analysis indicated that the coefficient of static friction and the coefficient of rolling friction between peanut straws were the most significant factors affecting the angle of repose. Conversely, the coefficient of restitution did not significantly impact the angle of repose. By employing response surface optimization, the optimal combination of contact parameters was determined: the coefficients of restitution between stem-stem, static friction coefficient, and rolling friction coefficient were set to 0.23, 0.67, and 0.30, respectively, while the remaining contact parameters were assigned intermediate values (stem-film set to 0.30, 0.60, and 0.20 respectively; film-film set to 0.20, 0.71, and 0.65, respectively).

4) A combination of physical and simulation tests was utilized to verify the accuracy of the calibrated peanut seedling film contact parameters. Secondary simulation tests were performed under the optimal parameter combination conditions. Results indicated that

the error between the simulation and physical test results for the rest angle was 1.37%. The simulated values of the angle of repose closely matched the physical test values, demonstrating the effectiveness and feasibility of the intrinsic parameters of peanut seedling membrane and the calibrated contact parameters. These findings offer theoretical and data support for the discrete element simulation of peanut seedling membrane separation.

Acknowledgements

This work was financially supported by the National Natural Science Foundation of China (Grant No. 52175238), the Xinjiang Key Research and Development Program (Grant No. 2022B02022-1), the Engineering Research and Development of High-efficiency Intelligent Residue Film Recycling Equipment in 2022 (Second Batch) (Grant No. CEIEC-2022-ZM02-0226), and the Integrated Pilot Project for Research, Development, Manufacturing, and Promotion of Agricultural Machinery in Shandong Province (Grant No. NJYTHSD-202321).

[References]

[1] Yu Z Y, Hu Z C, Cao M Z, Wang S Y, Zhang P, Peng B L. Design of cleaning device of tangential flow and whole-feed peanut combine harvester. Transactions of the CSAE, 2019; 35(9): 29–37. (in Chinese)

[2] Zheng B, Tang M, Tang W, Yu G Y, Zeng J Q. Research progress of peanut meal and peanut straw in animal feeding. China Feed, 2023; 5: 152–162. (in Chinese)

[3] Wang Q D, Zhao J Y, Zhao L P, Zhang Z X, Dong W Z, Wang R X. Analysis of the feeding quality of peanut vine of 14 cultivars. China Feed, 2019; 07: 75–78. (in Chinese)

[4] Yang M, Zhang Y H, Zhang C, Gu F W, Yu Z Y, Hu Z C. Design and experiment of fan-sieve combined peanut film-seedling separating device based on shredding and separating. Transactions of the CSAM, 2020; 51(12): 112–121. (in Chinese)

[5] Liao Y T, Wang Z T, Liao Q X, Wang W Y, Zhou Y, Liang F. Calibration of discrete element model parameters of forage rape stalk at early pod stage. Transactions of the CSAM, 2020; 51(S1): 236–243. (in Chinese)

[6] Liu Y C, Zhang F W, Song X F, Wang F, Zhang F Y, Li X Z, et al. Study on mechanical properties for corn straw of double-layer bonding model based on discrete element method. Journal of Northeast Agricultural University, 2022; 53(1): 45–54. (in Chinese)

[7] Tian X L, Cong X, Qi J T, Guo H, Li M, Fan X H. Parameter calibration of discrete element model for corn straw - soil mixture in black soil areas. Transactions of the CSAM, 2021; 52(10): 100–108, 242. (in Chinese)

[8] Zhang X R, Hu X H, Liu J X, Yang Y M, Li Y. Calibration and verification of bonding parameters of banana straw simulation model based on discrete element method. Transactions of the CSAM, 2023; 54(5): 121–130. (in Chinese)

[9] Zhang T, Liu F, Zhao M Q, Ma Q, W W, Fan Q, et al. Determination of corn stalk contact parameters and calibration of discrete element method simulation. Journal of Northeast Agricultural University, 2018; 23(4): 120–127. (in Chinese)

[10] Zhao J K, Song W B, Li J J. Modeling and mechanical analysis of rice straw based on discrete element mechanical model. Chinese Journal of Soil Science, 2020; 51(5): 1086–1093. (in Chinese)

[11] Ma Z, Li Y M, Xu L Z. Discrete-element method simulation of agricultural particles' motion in variable-amplitude screen box. Computers and Electronics in Agriculture, 2015; 118: 92–99.

[12] Maraldi M, Molari L, Regazzi N, Molari G. Analysis of the parameters affecting the mechanical behaviour of straw bales under compression. Biosystems Engineering, 2017; 160: 179–193.

[13] Leblicq T, Smeets B, Vanmaercke S, Ramon H, Saeys W. A discrete element approach for modelling bendable crop stems. Computers and Electronics in Agriculture, 2016; 124: 141–149.

[14] Sadrmanesh V, Chen Y. Simulation of tensile behavior of plant fibers using the discrete element method (DEM). Composites Part A: Applied Science and Manufacturing, 2018; 114: 196–203.

[15] Kattenstroth R, Harms H-H, Lang T. Alignment of straw to optimise the cutting process in a combine's straw chopper. in: Proceedings of Land Technik AgEng, 2011; pp.354–357.

[16] Wu Z Y, Xie, F P, Mei Y R, Wang X S, Liu D W, Wu B. Review on calibration of discrete element method (DEM) parameters for agricultural engineering. Agriculture Engineering and Equipment, 2021; 48(4): 7–18. (in Chinese)

[17] Horabik J, Molenda M. Parameters and contact models for DEM simulations of agricultural granular materials: A review. Biosystems Engineering, 2016; 147: 206–225.

[18] Liu P, He J, Zhang Z Q, Lu C Y, Zhang Z G, Lin H. Kinematic characteristic analysis and field test of chopped stalk in straw retention machine based on CFD DEM coupling simulation method. Transactions of the CSAM, 2020; 51(S1): 244–253. (in Chinese)

[19] Niu Z Y, Kong X R, Shen B S, Li H C, Geng J, Liu J. Parameters calibration of discrete element simulation for pellet feed attrition. Transactions of the CSAM, 2022; 53(7): 132–140. (in Chinese)

[20] Markauskas D, Kačianauskas R. Investigation of rice grain flow by multi-sphere particle model with rolling resistance. Granular Matter, 2011; 13: 143–148.

[21] Wang L J, Chai J, Wang H S, Wang Y S. Design and performance of a countersunk screen in a maize cleaning device. Biosystems Engineering, 2021; 209: 300–314.

[22] Bao Q J. Kinematic analysis and Simulation of dry peanut cleaning characteristics and screening device. Master dissertation. Shenyang: Shengyang Agricultural University, 2018; 50p. (in Chinese)

[23] Yang M. Study on separation technology and mechanism optimization of fan-sieve combined peanut residual film-seedling separating machine. Master dissertation. Beijing: Chinese Academy of Agricultural Sciences, 2021; 48p. (in Chinese)

[24] Hu G M. Analytical simulation of particulate systems by the discrete element method: Industrial applications of the discrete element method and introduction to EDEM software. Wuhan: Wuhan University of Technology Press. 2010; 11p.

[25] Wang G Q, Hao W J, Wang J X. Discrete unit method and its practice on EDEM. Xi'an: Xi'an University of Technology Press. 2010; 155p.

[26] Roessler T, Katterfeld A. DEM parameter calibration of cohesive bulk materials using a simple angle of repose test. Particuology, 2019; 45: 105–115.

[27] Roessler T, Katterfeld A. Scaling of the angle of repose test and its influence on the calibration of DEM parameters using upscaled particles. Powder Technology, 2018; 330: 58–66.

[28] Coetzee C J. Calibration of the discrete element method and the effect of particle shape. Powder Technology, 2016; 297: 50–70.

[29] Combarros M, Feise H J, Zetzener H, Kwade A, et al. Segregation of particulate solids: Experiments and DEM simulations. Particuology, 2014; 12: 25–32.

[30] Surdilovic J, Praeger U, Herold B, Truppel I, Geyer M. Impact characterization of agricultural products by fall trajectory simulation and measurement. Computers and Electronics in Agriculture, 2018; 151: 460–468.

[31] Wu T, Huang W F, Chen X S, Ma X, Han Z Q, Pan T. Calibration of discrete element model parameters for cohesive soil considering the cohesion between particles. Journal of South China Agricultural University, 2017; 38(3): 93–98. (in Chinese)

[32] Liu C L, Wei D, Song J N, Li Y N, Du X, Zhang F Y. Systematic study on boundary parameters of discrete element simulation of granular fertilizer. Transactions of the CSAM, 2018; 49(9): 82–89. (in Chinese)

[33] Liang R Q, Chen X G, Zhang B C, Wang X Z, Kan Z, Meng H W. Calibration and test of the contact parameters for chopped cotton stems based on discrete element methon. Int J Agric & Biol Eng, 2022; 15(5): 1–8.

[34] Peng F, Wang H Y, Fang F, Liu Y D. Calibration of discrete element model parameters for pellet feed based on injected section method. Transactions of the CSAM, 2018; 49(4): 140–147. (in Chinese)